ACS APPLIED MATERIALS & INTERFACES

Research Article

www.acsami.org

Catalase Mimic Property of Co_3O_4 Nanomaterials with Different Morphology and Its Application as a Calcium Sensor

Jianshuai Mu,[†] Li Zhang,[†] Min Zhao,[‡] and Yan Wang*[,†]

[†]Academy of Fundamental and Interdisciplinary Sciences, Harbin Institute of Technology, Harbin 150001, China

[‡]College of Life Science, Northeast Forestry University, Harbin 150040, China

Supporting Information

ABSTRACT: The applications of inorganic nanomaterials as biomimetic catalysts are receiving much attention because of their high stability and low cost. In this work, Co_3O_4 nanomaterials including nanoplates, nanorods, and nanocubes were synthesized. The morphologies and compositions of the products were characterized by scanning electron microscopy, transmission electron microscopy, and X-ray diffraction. The catalytic properties of Co_3O_4 nanomaterials as catalase mimics were studied. The Co_3O_4 materials with different morphology exhibited different catalytic activities in the order of nanoplates > nanorods > nanocubes. The difference of the catalytic activities originated from their different abilities of electron transfer. Their catalytic activities increased significantly in the presence of calcium ion. On the basis of the stimulation by calcium ion, a biosensor was constructed by Co_3O_4 nanoplates for the determination of calcium ion. The biosensor had a linear relation to calcium concentrations and good measurement correlation between 0.1 and 1 mM with a detection limit of 4 μM (S/N = 3). It showed high selectivity against other metal ions and good reproducibility. The proposed method was successfully applied for the determination of calcium in a milk sample.

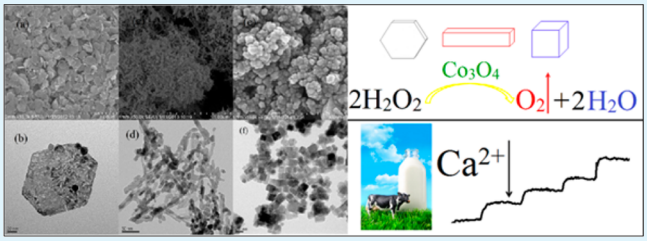

KEYWORDS: *nanomaterials, catalase mimic, morphology effect, amperometric biosensor, calcium determination*

1. INTRODUCTION

Hydrogen peroxide is a byproduct of normal oxygen metabolism that can cause oxidative damage to macromolecules in biological cells.[1] Catalases present in all aerobic organisms and many anaerobic organisms can catalyze the decomposition of hydrogen peroxide to molecular oxygen and water; therefore, they are protective enzymes.[2] These enzymes thus act as antioxidants by protecting cells against the damaging effects. The damages are linked to several diseases and disorders, including Parkinson's and Alzheimer's disease, cardiovascular disease, and even tumor development.[3] As biological catalysts, catalases have remarkable advantages such as highly efficient and selective catalysis under mild conditions. However, the natural enzymes own several drawbacks including low stability, high cost, and so on. Therefore, an attempt to develop stable and efficient mimics of catalase is very useful for various applications.[4−6]

Recently, inorganic nanomaterials as enzyme mimics have received increasing attention because of their several distinct properties, such as abundance of reactive groups on their surfaces for further functionalization and more catalytic sites on their surface than their bulk counterparts.[7−19] So far, most reported nanomaterials as artificial enzymes were mainly peroxidase mimics, and they were successfully applied to a variety of analytical problems. However, only a few works reported the catalase mimic activity of nanomaterials, which included Pt nanoparticles,[20] cerium oxide nanoparticles,[21] RuO_2 nanoparticles,[22] Fe_3O_4 nanoparticles,[23] and Co_3O_4 nanoparticles.[24] The factors influencing the catalase mimic activities of nanomaterials have not been reported, and the applications of these catalase mimics have been rarely studied. The catalytic performance of these nanomaterials as catalase mimics might be closely associated with their morphology. This inspired us to carry out a study that might help to understand the influence of morphology on their catalytic activities and then exploit more useful biomimetic catalysts with high catalytic activity.

It had been reported that the activity of catalase varied in the presence of some small molecules because of the interaction between enzyme molecules and the small molecules present in the enzyme surroundings.[25,26] The small molecules might be products of normal metabolic processes or normal constituents of tissues such as metal ions. For example, based on the variation of enzymes' activity by these small molecules, the enzyme electrodes were applied in the biosensor field for detecting a metal ion or biochemical molecule.[27−29]

In this work, Co_3O_4 nanoplates, nanorods, and nanocubes were synthesized, and then the influence of morphology on their catalase mimic activity was studied. Furthermore, calcium ion was found to enhance significantly the catalytic activities of Co_3O_4 nanomaterials, and based on the stimulation, an

Received: December 30, 2013
Accepted: May 5, 2014
Published: May 5, 2014

amperometric sensor was constructed for the determination of calcium in milk.

2. EXPERIMENTAL SECTION

2.1. Materials. $Co(NO_3)_2{\cdot}6H_2O$, $Co(CH_3COO)_2{\cdot}4H_2O$, $CoCl_2{\cdot}6H_2O$, hexamethylenetetramine, sodium hydroxide, ethylene glycol, sodium carbonate, ammonium hydroxide, and hydrogen peroxide were purchased from Sinopharm Chemical Reagent Co. (Shanghai, China). 3,3′,5,5′-Tetramethylbenzidine (TMB, ≥99%) and 5,5-dimetheyl-1-pyrroline *N*-oxide (DMPO, ≥99%) were obtained from Sigma-Aldrich (St. Louis, USA). The other metal salts for detection including calcium carbonate (primary reagent), sodium chloride, potassium chloride, nickel(II) chloride hexahydrate, magnesium chloride hexahydrate, zinc chloride, iron(III) chloride hexahydrate, and manganese(II) chloride tetrahydrate were obtained from Sinopharm Chemical Reagent Co. (Shanghai, China). All chemicals were of analytical grade apart from that mentioned above and used as received without further purification. Three kinds of milks with different brands were purchased from a market.

2.2. Preparation of Co_3O_4 Nanomaterials. Co_3O_4 nanoplates were synthesized according to the reported route.[30] First, 1.3 g of $Co(NO_3)_2{\cdot}6H_2O$ was dissolved in 100 mL of water and mixed with 100 mL of solution containing 0.6 g of hexamethylenetetramine (HMTA), under continuous stirring. A few drops of 1 M NaOH solution were then added in the above solution to obtain pH 10. Then, the solution was vigorously stirred for 2 h, and the solution was then transferred into the autoclaves, sealed, and maintained at 110 °C for 15 h. After these processes, the autoclaves were naturally cooled to room temperature, and the synthesized products were washed with water, ethanol, and acetone sequentially and dried at room temperature. The synthesized products were then calcined at 200 °C for 2 h.

The Co_3O_4 nanorods were prepared according to the method reported in the literature.[31] An amount of 1.66 g of $Co(CH_3COO)_2{\cdot}4H_2O$ was dissolved in 20 mL of ethylene glycol, and the solution was gradually heated to 160 °C. At a continuous flow of nitrogen, 67 mL of aqueous 0.2 M sodium carbonate solution was added at the rate of 1.1 mL min^{-1} under vigorous stirring. Then the slurry was further stirred and aged for 1 h. After centrifugation, the solid was washed with water, dried at 50 °C overnight under vacuum, and then calcined at 450 °C for 4 h in air.

The Co_3O_4 nanocubes were synthesized according to the literature.[9] Briefly, 0.50 g of $Co(CH_3COO)_2{\cdot}4H_2O$ was dissolved in the solution of 10 mL of water and 15 mL of ethanol. Under vigorous stirring, 2.5 mL of 25% ammonia was added drop by drop to the above solution. The solution was stirred for about 15 min in air, snd the solution was transferred into an autoclave with 48 mL volume, sealed, and heated to 150 °C for 3 h. Then, the autoclave was cooled to room temperature naturally. The black products were obtained by centrifugation, washed with water several times, and dried at 60 °C overnight under vacuum.

2.3. Preparation of Co_3O_4 Nanomaterials Modified Electrodes. Before the glassy carbon electrode (GCE, 3.0 mm diameter) surface modification, the electrodes were polished with 0.3 μm and 0.05 μm alumina slurry and then washed ultrasonically in water and ethanol, successively. The three Co_3O_4 nanomatetials were dispersed into distilled water by ultrasonic dispersion to obtain the three suspensions of Co_3O_4 nanomaterials (3 mg mL^{-1}), and three colloidal solutions (5 μL) were then dropped on three pretreated GCE surfaces and allowed to dry at 70 °C. Then, an aliquot of 2 μL of nafion solution (0.5 wt %) was casted on the layer of Co_3O_4 nanomatetials and dried at 70 °C.

2.4. Preparation of Milk Sample. Amounts of 5 mL of milk and 50 mL of HNO_3:$HClO_4$ (5:1 v/v) were placed in a beaker which was closed and left overnight. The temperature of this mixture was slowly increased, using a hot-plate, until fumes of acids appeared. This solution was evaporated almost completely, transferred, and adjusted to 50 mL in a flask with milli-Q water. The concentrations were first obtained by inductively coupled plasma atomic emission spectroscopy (ICP-AES) with an Optima 8000 ICP-OES spectrometer (PerkinElmer, USA).

2.5. Characterization of Co_3O_4 Nanomaterials with Different Morphologies. The composition and phase of the Co_3O_4 nanomaterials were obtained by powder X-ray diffraction (XRD) with a X-ray diffractometer (Rigaku, Japan) using Cu Kα radiation (λ = 1.5418 Å). The size and morphology of the Co_3O_4 nanomaterials were measured by scanning electron microscopy (SEM) with a SU-8000 SEM (Hitachi, Japan) and transmission electron microscope (HRTEM, Tecnai G2 F30, USA).

2.6. Catalytic Experiments and Electrochemical Measurements. The catalytic activities of the Co_3O_4 nanomaterials as catalase mimics were examined in NaH_2PO_4–NaOH buffer (3 mL, 100 mM, pH 9.0) containing Co_3O_4 nanomaterials (20 μg mL^{-1}), in the presence of H_2O_2. The concentrations of H_2O_2 were monitored in time-drive mode at 240 nm by using a Lambda 750 UV–Vis–NIR spectrophotometer (Perkin Elmer, American). The effect of pH on the catalytic activities of the Co_3O_4 nanomaterials was measured in 3 mL of 100 mM phosphate buffer (different pHs) containing Co_3O_4 nanomaterials (20 μg mL^{-1}) and 20 mM H_2O_2. The absorbance of reaction solutions was monitored at 240 nm. The reaction time was 20 min, and the variation of H_2O_2 concentration was calculated by its molar absorption coefficient of 39.4 M^{-1} cm^{-1} at 240 nm. The effect of temperature on the catalytic activities of the Co_3O_4 nanomaterials was examined in 3 mL of 100 mM NaH_2PO_4–NaOH buffer (pH 9.0) containing Co_3O_4 nanomaterials (20 μg mL^{-1}) and 20 mM H_2O_2 at different temperatures. The reaction time was 5 min.

The apparent steady-state reaction rates of three Co_3O_4 nanomaterials were deduced according to the initial linear range of the kinetic curves and the molar absorption coefficient of 39.4 M^{-1} cm^{-1} for H_2O_2. The reaction rates were fitted to the Michaelis–Menten equation to calculate the kinetic constants: $v = V_{max} \times [S]/(K_m + [S])$, where v is the initial velocity, V_{max} the maximal reaction velocity, [S] the concentration of substrate H_2O_2, and K_m the Michaelis constant.

In the absence of calcium ion, the fluorescence spectra were obtained under the following conditions: 20 mM H_2O_2, 1 mM terephthalic acid and different concentrations of the Co_3O_4 nanomaterials in 100 mM pH 9.0 NaH_2PO_4–NaOH buffer exposed to UV light for 10 min at 365 nm. After centrifugation, the reaction solutions were measured by a LS55 fluorescence spectrophotometer (PerkinElmer, USA). Test conditions: E_x = 315 nm, E_x slit = 15 nm, E_m slit = 5 nm. In the presence of calcium ion, the fluorescence spectra were measured with 1 mM terephthalic acid, 20 mM H_2O_2, 40 μg mL^{-1} Co_3O_4 nanomaterials, and different concentrations of calcium ion in 100 mM sodium acetate–NaOH buffer (pH 9.0) exposed to UV light for 10 min at 365 nm. After centrifugation, the solutions were used for fluorometric measurement. Test conditions: E_x = 315 nm, E_x slit = 15 nm, E_m slit = 5 nm.

The electron spin resonance (ESR) measurements were carried out with an A200 ESR spectrometer (Bruker, Germany). The conditions were as followes: 20 mW microwave power, 1 G modulation amplitude, and 100 G scan range.

Cyclic voltammetry (CV) and amperometric measurements were measured with a CHI 660D (Chenhua, China). A three-electrode system comprising the Co_3O_4 nanomaterial-modified glassy carbon electrode (GCE) as working electrodes, an Ag/AgCl electrode as reference, and a platinum plate as auxiliary was used for the electrochemical experiments.

3. RESULTS AND DISCUSSION

3.1. Characterization of Co_3O_4 Nanomaterials. The morphology of synthesized Co_3O_4 nanomaterials was characterized by a scanning electron microscope and transmission electron microscope. The Co_3O_4 nanoplates are uniform, and their average edge length and thickness are 100 and 21 nm, respectively (Figure 1a and 1b). The Co_3O_4 nanorods have a diameter of about 10 nm and length ranging from 40 to 80 nm (Figure 1c and 1d). The average size of Co_3O_4 nanocubes is ~19 nm (Figure 1e and 1f). The crystal structures of the three Co_3O_4 nanomaterials were determined by X-ray powder

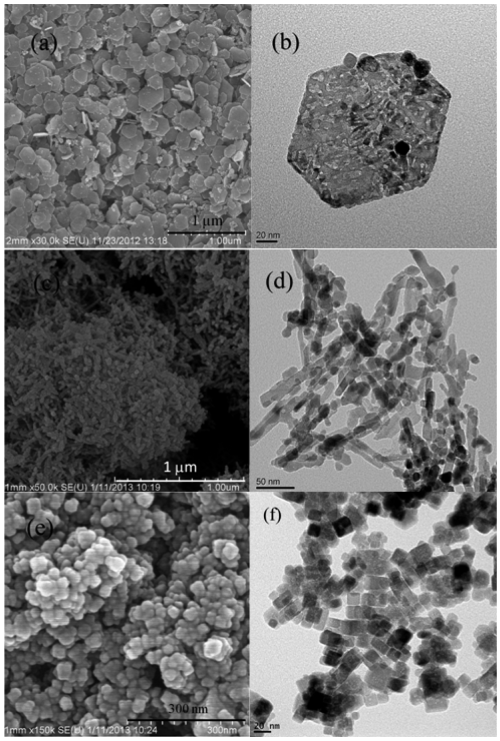

Figure 1. SEM images of Co_3O_4 nanoplates (a), nanorods (c), and nanocubes (e). TEM images of Co_3O_4 nanoplates (b), nanorods (d), and nanocubes (f).

diffraction (XRD). Despite variations in morphology, all the patterns could be indexed with the spinel structure of Co_3O_4 in good agreement with the reported data (JCPDS no. 76-1802).[32] No impurity peaks were observed, indicating the high purity of the three products (Figure 2).

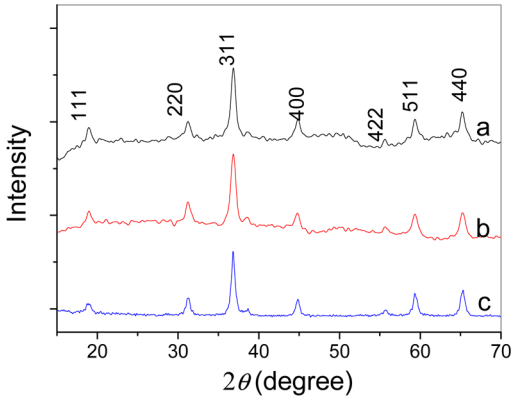

Figure 2. XRD patterns of (a) Co_3O_4 nanoplates, (b) Co_3O_4 nanrods, and (c) Co_3O_4 nanocubes.

3.2. Catalase Mimic Activity of Co_3O_4 with Different Morphology. To study the catalase mimic activity of Co_3O_4 nanomaterials, experiments were measured by using UV−vis spectrophotometry at 240 nm (the molar extinction coefficient of H_2O_2: ε_{240} = 39.4 M^{-1} cm^{-1}).[33] Similar to H_2O_2 decomposition by catalase, when the Co_3O_4 nanomaterials were incubated with H_2O_2 as the sole substrate, the decomposition of H_2O_2 was observed over reaction time (Figure 3a), and the three Co_3O_4 nanomaterials exhibited different levels of catalytic activity, following the order of nanoplates > nanorods > nanocubes.

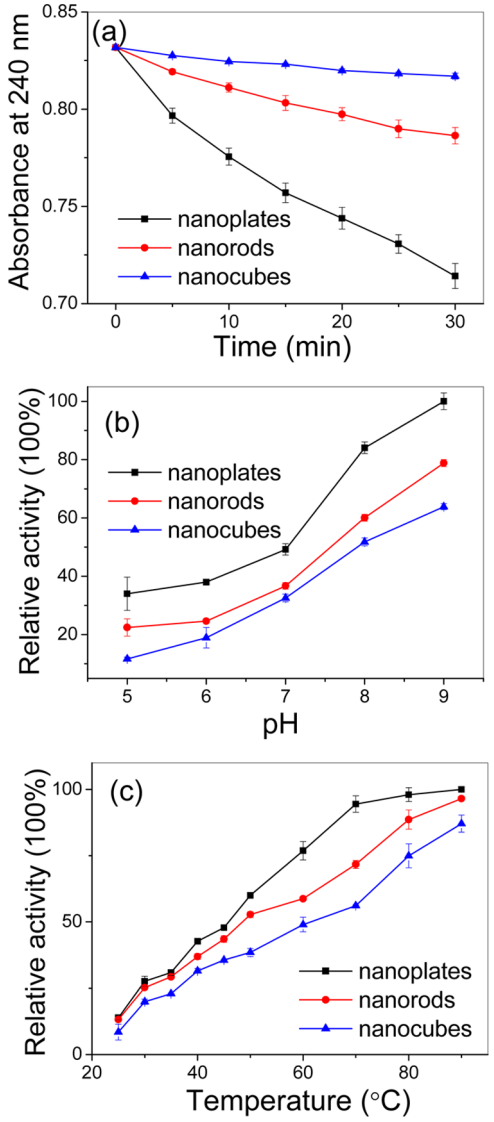

Figure 3. Decomposition of H_2O_2 by Co_3O_4 nanoplates, nanorods, and nanocubes (a), and effects of pH (b) and temperature (c) on the catalytic activity of Co_3O_4 nanoplates, Co_3O_4 nanorods, and Co_3O_4 nanocubes. (a, c) 20 mM H_2O_2, 20 μg mL^{-1} Co_3O_4 nanomaterials, 100 mM NaH_2PO_4−NaOH buffer (pH 9.0). (b) 20 mM H_2O_2, 20 μg mL^{-1} Co_3O_4 nanomaterials, 100 mM phosphate buffer (different pHs). The reaction time was 20 min. (c) The reaction time was 5 min. (b, c) The maximum point was set as 100%.

The effect of external conditions was investigated to understand the origin of different catalytic activities. The catalytic activities were measured varying the pH from 5 to 9 and the temperature from 25 to 90 °C. As shown in Figure 3b, the catalase mimic activity of the three Co_3O_4 nanomaterials continued to increase as the pH was raised. The reason was that H_2O_2 could dissociate into the perhydroxyl anion (OOH^-) more easily at a higher pH.[34] The OOH^- was more nucleophilic than H_2O_2 and could react with the metal centers of Co_3O_4 nanomaterials more easily. Therefore, the rates of the two reactions increased at a higher pH, thus accelerating the catalytic process of H_2O_2 decomposition by Co_3O_4 nanoma-

dx.doi.org/10.1021/am406033q | ACS Appl. Mater. Interfaces 2014, 6, 7090−7098

terials, and their catalytic activities all increased with increasing temperature in the investigated range (Figure 3c). The three Co_3O_4 nanomaterials as catalase mimics owned the same optimal pH (pH 9) and temperature (90 °C) in the investigated range. These results showed that the different catalytic activities of Co_3O_4 nanomaterials were not associated with the external conditions but their different morphology.

3.3. Catalytic Kinetics of Co_3O_4 Nanomaterials. The catalytic properties of the Co_3O_4 nanomaterials were further investigated using steady-state kinetics. The details of the catalytic performance were fitted by the classical Michaelis–Menten model.[7] The kinetic data of Co_3O_4 nanomaterials were measured by varying the concentration of H_2O_2 (Figure S1a–c, Supporting Information). The Lineweaver–Burk double reciprocal plots (Figure S1d–f, Supporting Information) showed the good linear relationship between v^{-1} and $[S]^{-1}$. The V_{max} and K_m of the three Co_3O_4 nanomaterials could be obtained by the slopes and intercepts of these lines. The experiment data were well fitted to the Michaelis–Menten equation to obtain the parameters shown in Table 1. The V_{max} values increased from nanocubes through nanorods to nanoplates. V_{max} values are the indicators of reaction activity (i.e., the rate of reaction when an enzyme is saturated with the substrate). The V_{max} values of the three Co_3O_4 nanomaterials showed that nanoplates had the highest catalase mimic activity, and nanorods exhibited medium activity, higher than nanocubes, which was consistent with the results in Figure 3a. On the other hand, the lowest K_m values with the two substrates were shown with the nanorods followed by the nanoplates and then the nanocubes. K_m values represent the affinity of the enzyme towards the substrate. The lower the K_m values, the greater the affinity. The K_m values of the three Co_3O_4 nanomaterials suggested nanorods had the highest affinity and nanoplates ranked the second place, both of which were higher than that of nanocubes. This showed that the substrate H_2O_2 was able to coordinate most easily with the metal centers of Co_3O_4 nanorods. The coordinative interaction between H_2O_2 and metal centers of Co_3O_4 nanorods might be so strong that the exchange rates were not high enough; therefore, the catalase mimic activity of Co_3O_4 nanorods was lower than that of Co_3O_4 nanoplates.

Table 1. Catalase-Like Kinetic Parameters of the Various Co_3O_4 Nanomaterials

catalyst	K_m/mM	$V_{max}/10^{-6}$ M s^{-1}	$K_{cat}/10^{-2}$ s^{-1}	E_a/kJ mol^{-1}
nanoplates	24.7	2.38	2.86	44.00
nanorods	4.82	1.89	2.27	52.28
nanocubes	63.9	1.23	1.48	63.75

The enzymes lower the energy barrier which must be surmounted before the reaction takes place; therefore, the activation energy (E_a) of the reaction catalyzed by the enzyme is smaller than that not catalyzed by enzymes. The catalytic decompositions of H_2O_2 by the Co_3O_4 nanomaterials were studied at different temperatures (Figure S2a–c, Supporting Information). These plots of log $[H_2O_2]_t$ vs time were linear, which indicated that the reactions catalyzed by Co_3O_4 nanomaterials followed first-order kinetics with respect to H_2O_2. The rate constants k at different temperatures could be calculated from the slopes of these curves, and then the activation energies of three Co_3O_4 nanomaterials were

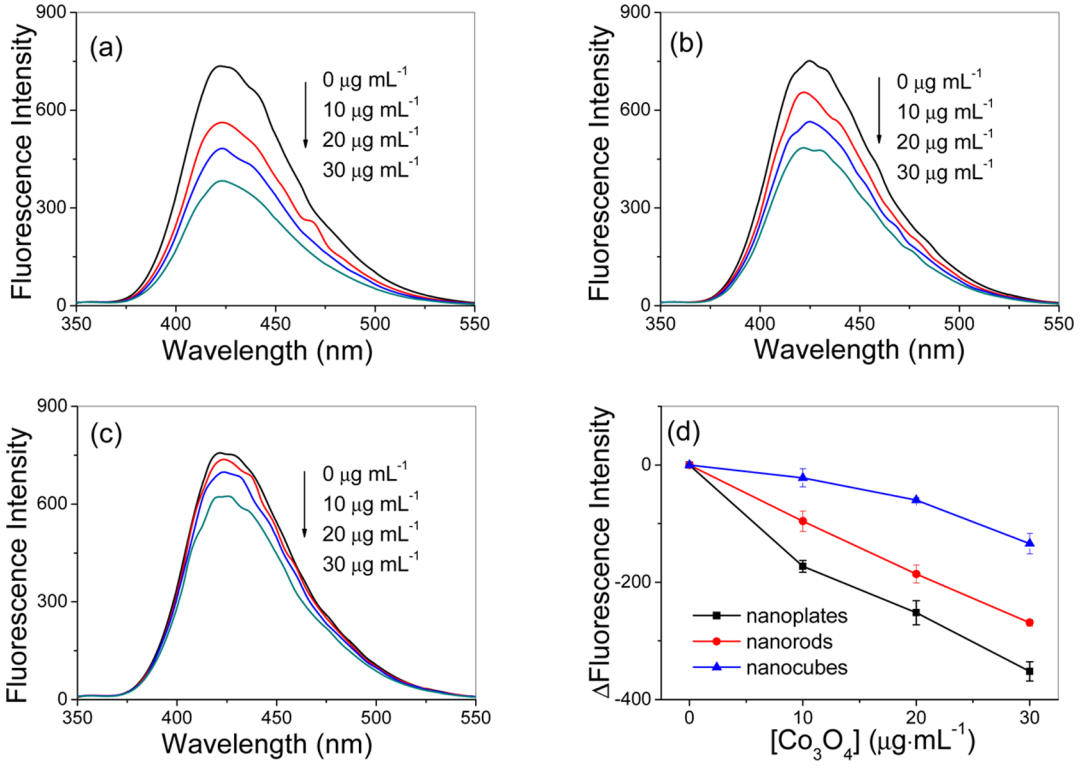

Figure 4. Effects of Co_3O_4 nanoplates (a), Co_3O_4 nanorods (b), and Co_3O_4 nanocubes (c) on the changes of hydroxyl radicals with terephthalic acid as a fluorescence probe and the comparison of hydroxyl radicals affected by the three Co_3O_4 nanomaterials (d). The samples containing 1 mM terephthalic acid, 20 mM H_2O_2, and different concentrations of the Co_3O_4 nanomaterials in 100 mM NaH_2PO_4–NaOH buffer (pH 9.0) were exposed to UV light for 10 min at 365 nm. After centrifugation, the solutions were used for fluorometric measurement.

calculated using the Arrhenius equation (Figure S 2d–f, Supporting Information). The three activation energies were all less than that of 210 kJ mol^{-1} for thermal decomposition of H_2O_2,[35] showing that the Co_3O_4 nanomaterials all lowered the energy barrier for H_2O_2 decomposition (Table 1). The E_a of the Co_3O_4 nanomaterials followed the order: nanoplates < nanorods < nanocubes. This indicated that the three Co_3O_4 nanomaterials owned different activities of lowering the energy barrier, which influenced their different catalase mimic activities.

To investigate whether hydroxyl radicals took part in the catalytic decomposition of H_2O_2 by Co_3O_4 nanomaterials, the fluorescent probe (terephthalic acid) was chosen to evaluate the production of hydroxyl radical by Co_3O_4 nanomaterials.[9] Hydroxyl radical can react readily with terephthalic acid, forming highly fluorescent 2-hydroxy terephthalic acid that can be identified from a fluorescence spectrometer. The three Co_3O_4 nanomaterials all reduced the hydroxyl radical production in a concentration-dependent manner (Figure 4). The ESR technique was also employed to prove the changes of hydroxyl radicals affected by Co_3O_4 nanomaterials. The intensity of the ESR signal decreased with addition of Co_3O_4 nanomaterials (Figure S3a, Supporting Information). As shown in Figure 4 and Figure S3a (Supporting Information), the decreases of hydroxyl radicals exhibited the order: nanoplates > nanorods > nanocubes. The order was consistent with that of their catalytic activity. This indicated that Co_3O_4 nanomaterials reduced the formation of hydroxyl radicals through catalyzing the decomposition of H_2O_2. The reason was that the concentrations of H_2O_2 decreased with addition of Co_3O_4 nanomaterials, reducing the concentrations of hydroxyl radicals which were derived from the H_2O_2 self-decomposition. The results of fluorescence experiments and ESR experiments all showed that there was no formation of hydroxyl radicals during the catalytic decomposition course of H_2O_2 by Co_3O_4 nanomaterials.

One molecule of H_2O_2 can oxidize the metal center of natural catalase to an oxidation state and generates water, and then the second hydrogen peroxide is used as a reductant of the oxidation state enzyme to regenerate the resting state enzyme, water, and oxygen.[36] Therefore, the natural catalase can transfer electrons from one molecule of H_2O_2 to another H_2O_2. As a kind of semiconductor material, Co_3O_4 nanomaterials might act as electron transfer mediators, similar to natural catalase.[37] The redox potential of O_2/H_2O_2 (equation 1 in Scheme 1) in the reaction systems of this work could be calculated to be 0.200 V using the Nernst equation (Table S1, Supporting Information). The redox potential of H_2O_2/OH^- (equation 2 in Scheme 1) was also calculated to be 1.126 V (Table S1, Supporting Information). As shown in Figure S4 (Supporting Information), the redox potentials of Co(III)/Co(II) for Co_3O_4 nanoplates, nanorods, and nanocubes were 1.095, 1.103, and 1.108 V, respectively (plus the potential of Ag/AgCl electrode, 0.200 V). According to the redox potentials of O_2/H_2O_2, Co(III)/Co(II), and H_2O_2/OH^-, first, the Co(III) of Co_3O_4 nanomaterials could get electrons easily from H_2O_2 and turned into Co(II), making H_2O_2 oxidized into oxygen and water. Secondly, the Co(II) of Co_3O_4 nanomaterials could pass electrons to H_2O_2 and turned back to Co(III), making H_2O_2 reduced to OH^- (Scheme 1). Co_3O_4 nanoplates with the lowest redox potential could pass electrons to H_2O_2 more easily than nanorods and nanocubes. Because the cleavage of the O–O bond (the reduction of H_2O_2) was the rate-determining step in the catalytic cycles,[38] Co_3O_4 nanoplates exhibited the highest catalase-like activity in the three Co_3O_4 nanomaterials. The currents of Co_3O_4 nanomaterials followed the order nanoplates > nanorods > nanocubes, showing the different electron transfer rates of the three Co_3O_4 nanomaterials (Figure S4, Supporting Information). The different electron transfer abilities of Co_3O_4 nanomaterials explained why their catalase-like activities exhibited the order: nanoplates > nanorods > nanocubes.

Scheme 1. Possible Mechanism of Co_3O_4 Nanomaterials As Catalase Mimics

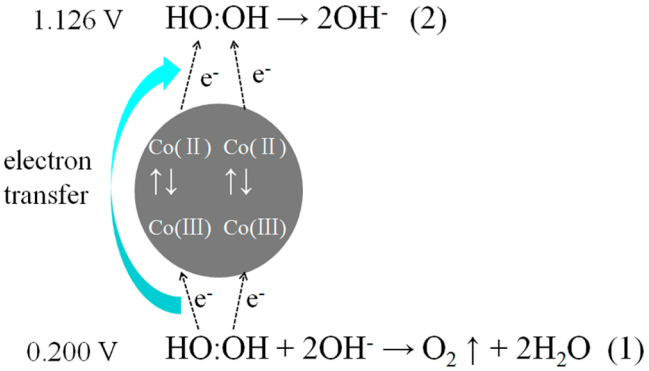

3.4. Stimulation of Catalytic Activity by Calcium Ion. It was well known that some small molecules present in the enzyme surroundings could inhibit or enhance the activity of enzyme. For example, calcium ion stimulated the catalytic activity of plant catalase and down-regulated the H_2O_2 levels.[25] As shown in Figure 5, the decomposition of H_2O_2 by Co_3O_4 nanomaterials increased significantly when calcium ion was added into the reaction system. This showed that calcium ion stimulated the catalytic activities of Co_3O_4 nanomaterials, similar to natural catalase. The calcium ion itself did not own the catalytic activity (data not shown); therefore, the enhancements arose from the synergistic effect between calcium ion and Co_3O_4 nanomaterials, and different Co_3O_4 nanomaterials exhibited different enhancements in the order of nanoplates > nanorods > nanocubes. As shown in Figure S5 (Supporting Information), the fluorescence intensity which represented the hydroxyl radical production all decreased as the concentration of calcium ion increased in the presence of three Co_3O_4 nanomaterials, and the decreases of fluorescence intensity with addition of Ca^{2+} followed the order: nanoplates > nanorods > nanocubes. The fluorescence results were also verified by ESR experiments. As shown in Figure S3b (Supporting Information), Ca^{2+} alone reduced hydroxyl radicals not evidently, but Ca^{2+} in the presence of Co_3O_4 nanomaterials decreased much more hydroxyl radical, compared with Co_3O_4 nanomaterials alone. The ESR results were consistent with that of fluorescence results. The results indicated that calcium ion promoted the catalytic decomposition of H_2O_2 by Co_3O_4 nanomaterials, thus reducing the formation of hydroxyl radicals. To explain that the catalytic activities of Co_3O_4 nanomaterials increased significantly in the presence of calcium ion, the electrochemistry of GCE modified by Co_3O_4 nanomaterials had been studied. The reduction currents of H_2O_2 increased when calcium ion was added in the reaction medium, and the increases of the three Co_3O_4 nanomaterials modified GCE were different (Figure S6a, Supporting Information). The reduction currents at −0.8 V increased steeply to reach a steady-state

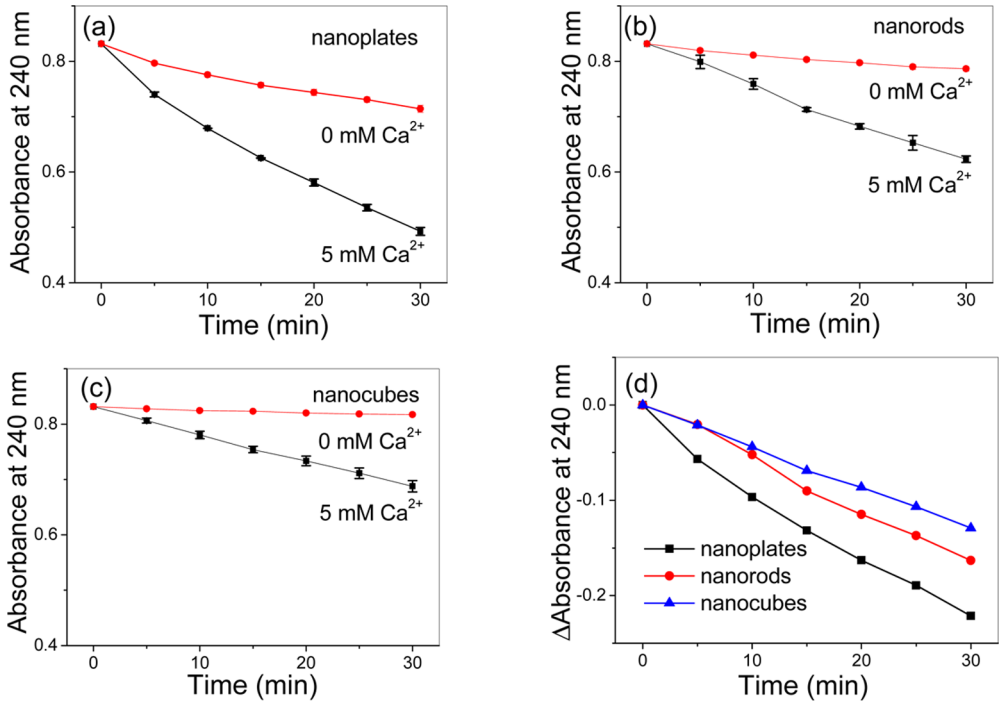

Figure 5. Effect of Ca^{2+} on the catalytic activities of Co_3O_4 nanoplates (a), nanorods (b), and nanocubes (c) as catalase mimics and the comparison of enhancements on the catalytic activities of different Co_3O_4 nanomaterials by Ca^{2+} (d). 20 mM H_2O_2 and 20 μg mL^{-1} Co_3O_4 nanomaterials in 100 mM NaH_2PO_4–NaOH buffer (pH 9.0) without Ca^{2+} or with 5 mM Ca^{2+}.

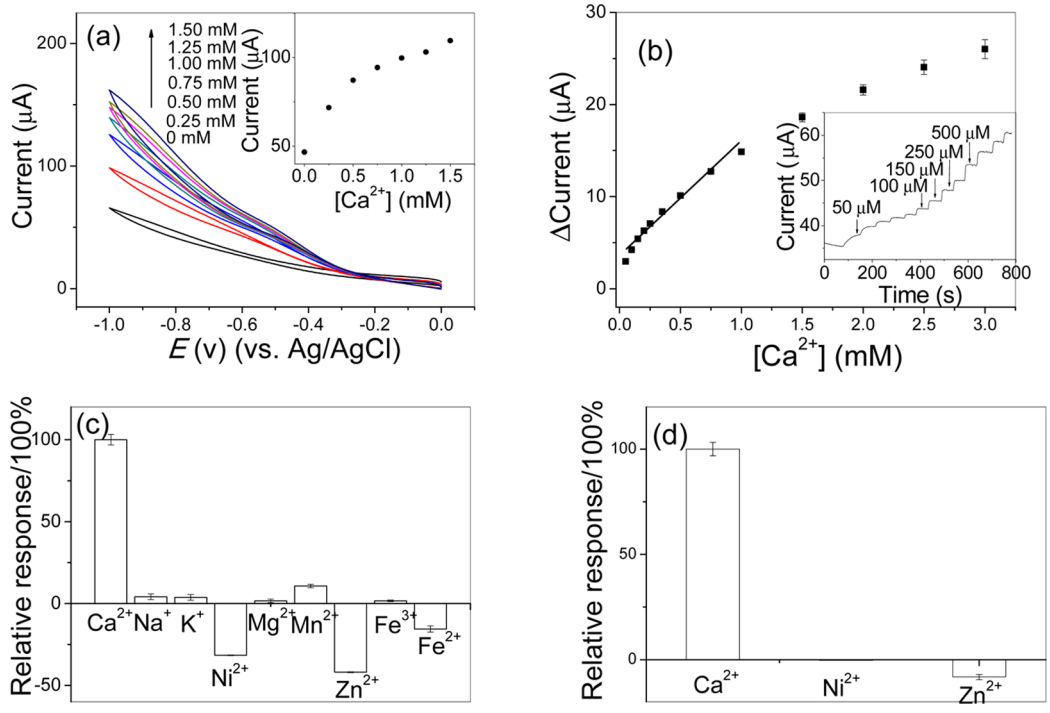

Figure 6. (a) Cyclic voltammograms of Co_3O_4 nanoplate modified electrodes in the presence of different concentrations of Ca^{2+}. The inset shows the variations of reduction current at −0.80 V. (b) Dose−response curve for detection of calcium ion. The inset shows the corresponding amperometric responses of the Co_3O_4 nanoplate electrode upon the successive addition of Ca^{2+}. The curve was measured 5 times. (c) The response of the Co_3O_4 nanoplate electrode with the addition of Ca^{2+} and other interfering metal ions at the same concentrations. (d) The response of the Co_3O_4 nanoplate electrode with the addition of Ca^{2+} and other interfering metal ions at the concentration ratio of 10:1. 5 mM H_2O_2 in 100 mM Tris-HCl buffer (pH 9.0). (c) The concentration of all metal ions was 0.5 mM. (d) The concentration of Ca^{2+} was 0.5 mM, and the concentration of Ni^{+} and Zn^{2+} was 0.05 mM. (c,d) The response of 0.5 mM Ca^{2+} was set as 100%.

value with addition of an aliquot of Ca^{2+} (Figure S6b, Supporting Information). The three Co_3O_4 nanomaterials showed different increases of reduction currents, following the order of nanoplates > nanorods > nanocubes. This showed

Table 2. Determination of Calcium in Milk by Using the Biosensor and ICP-AES

samples	concentration[a]/mM (by biosensor)	RSD/%	recovery[a]/%	concentration[a]/mM (by ICP-AES)	RSD/%	recovery[a]/%
milk 1	24.6	3.9	98.6	26.0	0.4	99.7
milk 2	16.5	4.3	99.2	17.3	0.3	100.5
milk 3	17.8	4.5	99.1	18.9	0.5	100.3

[a]Mean value of three separate experiments using the biosensor.

Ca^{2+} could promote the electron transfer ability of Co_3O_4 nanomaterials, and the stimulations were different in the presence of different Co_3O_4 nanomaterials. This explained why calcium ion stimulated the catalytic activities of Co_3O_4 nanomaterials.

3.5. Application of Calcium Determination in Milk. Co_3O_4 nanomaterials modified GCE has been studied by electrochemistry to develop an amperometric biosensor for H_2O_2. The above experiments revealed that Co_3O_4 nanoplates exhibited the highest electrocatalytic activity with addition of Ca^{2+} in the three Co_3O_4 nanomaterials. Therefore, the Co_3O_4 nanoplates were chosen as the materials for the subsequent experiments.

To determine the effect of the pH value on the biosensor response, different buffer systems were used in the experiments. The optimum pH value was determined to be 9.0 in the investigated range (Figure S7, Supporting Information). Below this pH value, decreases in the biosensor responses were observed. This indicated that the immobilization on the electrode did not affect the optimum pH value of Co_3O_4 nanomaterials as catalase mimics (Figure 3b).

To determinate the effect of the H_2O_2 concentration on the biosensor response, different concentrations of H_2O_2 were used in the experiment. The current difference between reaction systems with and without Ca^{2+} increased as the H_2O_2 concentration increased and then decreased above 20 mM H_2O_2. The optimal concentration of H_2O_2 was determinate to be 20 mM. At a higher concentration of H_2O_2, the enhancement of electrocatalytic activity by Ca^{2+} decreased (Figure S8, Supporting Information). The reason was that a lot of formed oxygen bubbles during the H_2O_2 reduction were observed in the electrode and hindered the electrochemical reaction.

The electrocatalytic activity of the Co_3O_4 nanoplates modified electrode towards the reduction of H_2O_2 in the presence of Ca^{2+} was investigated. Figure 6a showed the CV responses containing various concentrations of Ca^{2+}. The reduction currents increased with the Ca^{2+} concentration, indicating that the Co_3O_4 nanoplates modified electrode could be applied for the detection of Ca^{2+}. As shown in the inset of Figure 6a, the increase gradually saturated at a high Ca^{2+} concentration.

Applied potentials of −0.80 V were chosen to conduct amperometric Ca^{2+} sensing. A well-defined, stable, and rapid change in current could be observed with the successive addition of Ca^{2+} (inset of Figure 6b). The Co_3O_4 nanoplates exhibited sensitive and rapid current response to the Ca^{2+} addition, achieving steady state current in about 20 s. The corresponding calibration curve of current versus concentration was presented (Figure 6b). The sensor displays a linear range from 0.1 to 1 mM. The calibration curve of current versus Ca^{2+} concentration was measured 5 times, and the maximum RSD during the linear range from 0.1 to 1 mM was 2.3%. This indicated that the modified GCE exhibited good reproducibility. With adding the calcium ion concentration of 5 μM, the amperometric response was triggered with a signal-to-noise ratio of ∼3.5 (Figure S9, Supporting Information). Therefore, the detection limit was estimated to be 4 μM (signal/noise = 3).

The proposed sensor was further applied to the determination of calcium in milk samples. The calcium concentrations of three milk samples with three different brands were measured and calibrated by the standard curve (Figure 6b). The experiments had been done three times to verify the reproducibility of the values (Table 2). The relative standard deviations (R.S.D.) were less than 5% for each milk sample, demonstrating good reproducibility of the Co_3O_4 nanoplate electrode. Milk samples were spiked with a similar standard concentration of Ca^{2+} as found in the samples themselves to ascertain exact results, and the recoveries were about 99%. The same milk sample was also measured by ICP-AES. This comparison clearly showed that our results agreed satisfactorily with those obtained by AES. The results implied the applicability of Co_3O_4 nanoplates modified electrode as a sensor for the determination of calcium in milk samples.

The selectivity of the sensor for Ca^{2+} was also investigated against some normally co-existing metal ions in the milk sample. Figure 6c showed the response of the Co_3O_4 nanoplate electrode for Ca^{2+} and other metal ions at the same concentrations. The results indicated that the responses for the addition of Na^+, K^+, Mg^{2+}, Mn^{2+}, Fe^{3+}, and Fe^{2+} were small compared to that of Ca^{2+}. However, the responses for Ni^{2+} and Zn^{2+} could not be neglected, and Ni^{2+} and Zn^{2+} had a negative impact on detection of Ca^{2+}, which indicated that they hindered the electrochemical process of the electrode. The major metal ion species in the milk sample included Ca^{2+}, Na^+, and K^+, while other metal ions were trace metal ions.[39] The concentrations of major metal ions were far higher than those of the trace metal ions. Therefore, the molar ratios of 1:10 between Ni^{2+} or Zn^{2+} and Ca^{2+} were also used to estimate their interference in the sensing of Ca^{2+}. Figure 6d showed the response of the Co_3O_4 nanoplate electrode for Ca^{2+} and Ni^{2+} or Zn^{2+} ions, at an applied potential of −0.8 V. It was to be noted that there were small responses for Ni^{2+} or Zn^{2+} ions. The responses could be neglected when compared to the response for the addition of Ca^{2+}. This implied that the sensor was suitable for the reliable determination of calcium in milk samples.

4. CONCLUSIONS

Co_3O_4 nanomaterials with different morphologies including nanoplates, nanorods, and nanocubes were synthesized. They exhibited different levels of catalase mimic activity, in the order of nanoplates > nanorods > nanocubes. The reactions catalyzed by the three Co_3O_4 catalysts were studied by the typical Michaelis−Menten model. The V_{max} values and K_{cat} values showed that nanoplates had the highest catalase mimic activity, and nanorods exhibited medium activity, higher than nanocubes, which was consistent with the above results. On the basis of the E_a of the three Co_3O_4 nanomaterials, they owned

different activities of lowering the energy barrier, which influenced their different catalase mimic activities. The above study showed morphology control of the three catalase mimics, providing the possibility to finely tune their catalytic activity. The catalytic activities of Co_3O_4 nanomaterials increased significantly in the presence of Ca^{2+}. On the basis of the stimulation, an amperometric biosensor with Co_3O_4 nanoplates was developed to detect Ca^{2+}. It exhibited low detection limit, high reproducibility, and good selectivity. The biosensor was then successfully used for the calcium determination of milk samples.

■ ASSOCIATED CONTENT

Supporting Information

Steady-state kinetic assay of Co_3O_4 nanomaterials (Figure S1); Kinetics of catalytic H_2O_2 decomposition by the Co_3O_4 nanomaterials at different temperatures (Figure S2); The effect of Co_3O_4 nanomaterials and Ca^{2+} in the presence of Co_3O_4 nanomaterials on the formation of hydroxyl radical detected by ESR (Figure S3); The redox potentials of O_2/H_2O_2 and H_2O_2/OH^- (Table S1); Cyclic voltammograms of electrodes modified by Co_3O_4 nanomaterials (Figure S4); The effect of Ca^{2+} on the formation of hydroxyl radicals in the presence of Co_3O_4 nanomaterials (Figure S5); The different enhancements on the electrocatalytic activities of three Co_3O_4 nanomaterials modified electrodes by Ca^{2+} (Figure S6); The enhancements on the electrocatalytic activities of Co_3O_4 nanoplates modified electrode by Ca^{2+} at different pHs (Figure S7); The enhancements on the electrocatalytic activities of Co_3O_4 nanoplates modified electrode by Ca^{2+} at different H_2O_2 concentrations (Figure S8); The amperometric response of Co_3O_4 nanoplates modified electrode to the addition of 5 μM Ca^{2+} (Figure S9). This material is available free of charge via the Internet at http://pubs.acs.org.

■ AUTHOR INFORMATION

Corresponding Author

*E-mail: wangy_msn@hit.edu.cn.

Notes

The authors declare no competing financial interest.

■ ACKNOWLEDGMENTS

This work was supported by the National Natural Science Foundation of China (No. 21273057).

■ REFERENCES

(1) Giorgio, M.; Trinei, M.; Migliaccio, E.; Pelicci, P. G. Hydrogen Peroxide: A Metabolic By-product or a Common Mediator of Ageing Signals? *Nat. Rev. Mol. Cell Biol.* **2007**, *8*, 722−728.

(2) Brioukhanov, A.; Netrusov, A. Catalase and Superoxide Dismutase: Distribution, Properties, and Physiological Role in Cells of Strict Anaerobes. *Biochemistry (Moscow)* **2004**, *69*, 949−962.

(3) Valko, M.; Leibfritz, D.; Moncol, J.; Cronin, M. T.; Mazur, M.; Telser, J. Free Radicals and Antioxidants in Normal Physiological Functions and Human Disease. *Int. J. Biochem. Cell Biol.* **2007**, *39*, 44−84.

(4) Fisher, A. E. O.; Maxwell, S. C.; Naughton, D. P. Catalase and Superoxide Dismutase Mimics for the Treatment of Inflammatory Diseases. *Inorg. Chem. Commun.* **2003**, *6*, 1205−1208.

(5) Triller, M. U.; Hsieh, W.-Y.; Pecoraro, V. L.; Rompel, A.; Krebs, B. Preparation of Highly Efficient Manganese Catalase Mimics. *Inorg. Chem.* **2002**, *41*, 5544−5554.

(6) Pessiki, P.; Khangulov, S.; Ho, D.; Dismukes, G. Structural and Functional Models of the Dimanganese Catalase Enzymes. 2. Structure, Electrochemical, Redox, and EPR Properties. *J. Am. Chem. Soc.* **1994**, *116*, 891−897.

(7) Gao, L.; Zhuang, J.; Nie, L.; Zhang, J.; Zhang, Y.; Gu, N.; Wang, T.; Feng, J.; Yang, D.; Perrett, S. Intrinsic Peroxidase-like Activity of Ferromagnetic Nanoparticles. *Nat. Nanotechnol.* **2007**, *2*, 577−583.

(8) André, R.; Natálio, F.; Humanes, M.; Leppin, J.; Heinze, K.; Wever, R.; Schröder, H. C.; Müller, W. E.; Tremel, W. V_2O_5 Nanowires with an Intrinsic Peroxidase-Like Activity. *Adv. Funct. Mater.* **2011**, *21*, 501−509.

(9) Mu, J.; Wang, Y.; Zhao, M.; Zhang, L. Intrinsic Peroxidase-like Activity and Catalase-like Activity of Co_3O_4 Nanoparticles. *Chem. Commun.* **2012**, *48*, 2540−2542.

(10) Song, Y.; Qu, K.; Zhao, C.; Ren, J.; Qu, X. Graphene Oxide: Intrinsic Peroxidase Catalytic Activity and its Application to Glucose Detection. *Adv. Mater.* **2010**, *22*, 2206−2210.

(11) Wang, X.-X.; Wu, Q.; Shan, Z.; Huang, Q.-M. BSA-stabilized Au Clusters as Peroxidase Mimetics for Use in Xanthine Detection. *Biosens. Bioelectron.* **2011**, *26*, 3614−3619.

(12) Zhang, Z.; Hao, J.; Yang, W.; Lu, B.; Ke, X.; Zhang, B.; Tang, J. Porous Co_3O_4 Nanorods−Reduced Graphene Oxide with Intrinsic Peroxidase-Like Activity and Catalysis in the Degradation of Methylene Blue. *ACS Appl. Mater. Interfaces* **2013**, *5*, 3809−3815.

(13) Dutta, A. K.; Maji, S. K.; Srivastava, D. N.; Mondal, A.; Biswas, P.; Paul, P.; Adhikary, B. Synthesis of FeS and FeSe Nanoparticles from a Single Source Precursor: A Study of their Photocatalytic Activity, Peroxidase-Like Behavior, and Electrochemical Sensing of H_2O_2. *ACS Appl. Mater. Interfaces* **2012**, *4*, 1919−1927.

(14) An, Q.; Sun, C.; Li, D.; Xu, K.; Guo, J.; Wang, C. Peroxidase-Like Activity of Fe_3O_4@ Carbon Nanoparticles Enhances Ascorbic Acid-Induced Oxidative Stress and Selective Damage to PC-3 Prostate Cancer Cells. *ACS Appl. Mater. Interfaces* **2013**, *5*, 13248−13257.

(15) Pautler, R.; Kelly, E. Y.; Huang, P.-J. J.; Cao, J.; Liu, B.; Liu, J. Attaching DNA to Nanoceria: Regulating Oxidase Activity and Fluorescence Quenching. *ACS Appl. Mater. Interfaces* **2013**, *5*, 6820−6825.

(16) He, W.; Wu, X.; Liu, J.; Hu, X.; Zhang, K.; Hou, S.; Zhou, W.; Xie, S. Design of AgM Bimetallic Alloy Nanostructures (M= Au, Pd, Pt) with Tunable Morphology and Peroxidase-like Activity. *Chem. Mater.* **2010**, *22*, 2988−2994.

(17) He, W.; Liu, Y.; Yuan, J.; Yin, J.-J.; Wu, X.; Hu, X.; Zhang, K.; Liu, J.; Chen, C.; Ji, Y. Au@ Pt Nanostructures as Oxidase and Peroxidase Mimetics for Use in Immunoassays. *Biomaterials* **2011**, *32*, 1139−1147.

(18) Heckert, E. G.; Karakoti, A. S.; Seal, S.; Self, W. T. The Role of Cerium Redox State in the SOD Mimetic Activity of Nanoceria. *Biomaterials* **2008**, *29*, 2705−2709.

(19) Asati, A.; Santra, S.; Kaittanis, C.; Nath, S.; Perez, J. M. Oxidase-Like Activity of Polymer-Coated Cerium Oxide Nanoparticles. *Angew. Chem., Int. Ed.* **2009**, *48*, 2308−2312.

(20) Kajita, M.; Hikosaka, K.; Iitsuka, M.; Kanayama, A.; Toshima, N.; Miyamoto, Y. Platinum Nanoparticle Is a Useful Scavenger of Superoxide Anion and Hydrogen peroxide. *Free Radical Res.* **2007**, *41*, 615−626.

(21) Pirmohamed, T.; Dowding, J. M.; Singh, S.; Wasserman, B.; Heckert, E.; Karakoti, A. S.; King, J. E. S.; Seal, S.; Self, W. T. Nanoceria Exhibit Redox State-dependent Catalase Mimetic Activity. *Chem. Commun.* **2010**, *46*, 2736−2738.

(22) Deng, H.; Shen, W.; Peng, Y.; Chen, X.; Yi, G.; Gao, Z. Nanoparticulate Peroxidase/Catalase Mimetic and its Application. *Chem.—Eur. J.* **2012**, *18*, 8906−8911.

(23) Chen, Z.; Yin, J.-J.; Zhou, Y.-T.; Zhang, Y.; Song, L.; Song, M.; Hu, S.; Gu, N. Dual Enzyme-like Activities of Iron Oxide Nanoparticles and their Implication for Diminishing Cytotoxicity. *ACS Nano* **2012**, *6*, 4001−4012.

(24) Mu, J. S.; Zhang, L.; Zhao, M.; Wang, Y. Co_3O_4 Nanoparticles as an Efficient Catalase Mimic: Properties, Mechanism and its Electrocatalytic Sensing Application for Hydrogen Peroxide. *J. Mol. Catal. A: Chem.* **2013**, *378*, 30−37.

(25) Yang, T.; Poovaiah, B. Hydrogen Peroxide Homeostasis: Activation of Plant Catalase by Calcium/calmodulin. *Proc. Natl. Acad. Sci. U.S.A.* **2002**, *99*, 4097−4102.
(26) Kimbrough, D. R.; Magoun, M. A.; Langfur, M. A Laboratory Experiment Investigating Different Aspects of Catalase Activity in an Inquiry-based Approach. *J. Chem. Educ.* **1997**, *74*, 210.
(27) Akbayirli, P.; Akyilmaz, E. Activation-Based Catalase Enzyme Electrode and its Usage for Glucose Determination. *Anal. Lett.* **2007**, *40*, 3360−3372.
(28) Akyilmaz, E.; Kozgus, O. Determination of Calcium in Milk and Water Samples by Using Catalase Enzyme Electrode. *Food Chem.* **2009**, *115*, 347−351.
(29) Akyilmaz, E.; Yorganci, E.; Novel, A. Biosensor Based on Activation Effect of Thiamine on the Activity of Pyruvate Oxidase. *Biosens. Bioelectron.* **2008**, *23*, 1874−1877.
(30) Hwang, S.; Umar, A.; Kim, S.; Al-Sayari, S.; Abaker, M.; Al-Hajry, A.; Stephan, A. M. Low-temperature Growth of Well-crystalline Co_3O_4 Hexagonal Nanodisks as Anode Material for Lithium-ion Batteries. *Electrochim. Acta* **2011**, *56*, 8534−8538.
(31) Xie, X.; Li, Y.; Liu, Z.-Q.; Haruta, M.; Shen, W. Low-temperature Oxidation of CO Catalysed by Co_3O_4 Nanorods. *Nature* **2009**, *458*, 746−749.
(32) Varghese, B.; Teo, C.; Zhu, Y.; Reddy, M. V.; Chowdari, B. V.; Wee, A. T. S.; Tan, V.; Lim, C. T.; Sow, C. H. Co_3O_4 Nanostructures with Different Morphologies and their Field-Emission Properties. *Adv. Funct. Mater.* **2007**, *17*, 1932−1939.
(33) Sun, H.; Gao, J.; Ferrington, D. A.; Biesiada, H.; Williams, T. D.; Squier, T. C. Repair of Oxidized Calmodulin by Methionine Sulfoxide Reductase Restores Ability to Activate the Plasma Membrane Ca-ATPase. *Biochemistry* **1999**, *38*, 105−112.
(34) Špalek, O.; Balej, J.; Paseka, I. Kinetics of the Decomposition of Hydrogen Peroxide in Alkaline Solutions. *J. Chem. Soc., Faraday Trans. 1* **1982**, *78*, 2349−2359.
(35) Hiroki, A.; LaVerne, J. A. Decomposition of Hydrogen Peroxide at Water-ceramic Oxide Interfaces. *J. Phys. Chem. B* **2005**, *109*, 3364−3370.
(36) Switala, J.; Loewen, P. C. Diversity of Properties among Catalases. *Arch. Biochem. Biophys.* **2002**, *401*, 145−154.
(37) Dong, J.; Song, L.; Yin, J.-J.; He, W.; Wu, Y.; Gu, N.; Zhang, Y. Co_3O_4 Nanoparticles with Multi-Enzyme Activities and its Application in Immunohistochemical Assay. *ACS Appl. Mater. Interfaces* **2014**, *6*, 1959−1970.
(38) Naruta, Y.; Sasayama, M.-A. Importance of Mn−Mn Separation and their Relative Arrangement on the Development of High Catalase Activity in Manganese Porphyrin Dimer Catalysts. *J. Chem. Soc., Chem. Commun.* **1994**, 2667−2668.
(39) Rodríguez Rodríguez, E.; Sanz Alaejos, M.; Díaz Romero, C. Mineral Concentrations in Cow's Milk from the Canary Island. *J. Food Compos. Anal.* **2001**, *14*, 419−430.